Available online at www.sciencedirect.com
SCIENCE DIRECT®
ELSEVIER
International Journal of Multiphase Flow 29 (2003) 1793–1816
International Journal of Multiphase Flow
www.elsevier.com/locate/ijmulflow

Evaluation of the equilibrium Eulerian approach for the evolution of particle concentration in isotropic turbulence

Sarma L. Rani [a,1], S. Balachandar [b,*]

[a] *Department of Mechanical and Industrial Engineering, University of Illinois at Urbana-Champaign, Urbana, IL 61801, USA*

[b] *Department of Theoretical and Applied Mechanics, 216 Talbot Lab., University of Illinois at Urbana-Champaign, Urbana, IL 61801, USA*

Received 9 November 2002; received in revised form 3 September 2003

Abstract

In the current work, the accuracy of the equilibrium Eulerian approach in evolving the particulate concentration field is evaluated by comparing it against the Lagrangian approach, for varying particle response time and terminal velocity. In particular, we compare the statistics of preferential accumulation and gravitational settling of particles in a cubic box of isotropic turbulence. Twelve simulations corresponding to four values of nondimensional particle response time, $\tau_p = 0.05, 0.1, 0.2, 0.4$, and three values of nondimensional terminal velocity, $|\mathbf{V}_s| = 0.5, 2, 4$ are considered. The equilibrium Eulerian approach obviates the need to solve additional governing equations for the particle velocity field. It, however, involves evolution of the particle concentration field using the equilibrium Eulerian velocity field. A spectral diffusion term is included in the particle concentration equation to provide an essentially non-oscillatory behavior to the solution. There is good agreement between the equilibrium Eulerian and Lagrangian statistics for small particles. With increasing particle size, the equilibrium Eulerian approach tends to somewhat overestimate particle preferential concentration in regions of excess strain-rate over rotation-rate compared to the Lagrangian approach. Over the entire range of parameters considered, the equilibrium approach provides a good approximation to the actual mean and rms fluctuating settling velocities of the particle.

* Corresponding author. Tel.: +1-217-244-4371; fax: +1-217-244-9090.
E-mail address: s-bala@uiuc.edu (S. Balachandar).
[1] Current address: Sibley School of Mechanical and Aerospace Engineering, Upson Hall, Cornell University, Ithaca, NY 14850, USA.

0301-9322/$ - see front matter © 2003 Published by Elsevier Ltd.
doi:10.1016/j.ijmultiphaseflow.2003.09.005

1. Introduction

Particle-laden flows are encountered in a wide range of natural as well as industrial situations such as pollutant dispersion in the atmosphere and oceans, dust deposition and removal in clean rooms, electrostatic precipitators, etc. The phenomena of interest in these processes are particle dispersion, preferential accumulation and mean settling of particles, etc.

Numerical simulations of particle-laden flows can be classified to be either Lagrangian or Eulerian according to the manner in which the disperse phase is treated. In the Lagrangian approach, trajectories and velocities of individual particles are computed by integrating the particle equations of motion. In the Eulerian approach, the particulate phase is also treated as a continuum much like the carrier phase. Conservation equations are developed for the mass and momentum of the particle phase and are solved to evolve the particulate phase velocity and concentration fields.

The Lagrangian and Eulerian approaches have their advantages as well as disadvantages. At high concentrations, it will be computationally taxing to track all the particles within the computational domain in the Lagrangian framework. Another difficulty with the Lagrangian approach is the lack of a rigorous way to incorporate the particle feedback to the fluid governing equations. The Eulerian treatment of the particulate phase provides a convenient framework in such scenarios. However, the Eulerian approach suffers from the disadvantage that additional set of partial differential equations must be solved for the particulate velocity and concentration fields. If particles of different sizes are simultaneously considered, the number of equations to be solved increases. Furthermore, the assumption of an Eulerian field for the particulate phase velocity is appropriate only for particles of sufficiently small size. However, the Eulerian momentum equations for the particulate phase become increasingly stiff as the particle size decreases, thus their solution is difficult to obtain for very small particles.

Recently, Ferry and Balachandar (2001), following earlier efforts by Maxey (1987) and Druzhinin (1995), Druzhinin and Elghobashi (1998, 1999), have explored the equilibrium approximation to the Eulerian velocity field of the particulate phase. In this approach, the particle velocity field, $\mathbf{v}(\mathbf{x},t)$, is expressed explicitly in terms of the fluid velocity field, $\mathbf{u}(\mathbf{x},t)$, as an expansion in particle response time. Thus, one avoids the need to solve additional momentum equations for the particulate phase velocity. With the equilibrium approximation, the velocity field corresponding to any number of particulate sizes can be easily obtained, provided their nondimensional time scale is sufficiently small for the equilibrium approximation to be appropriate. The velocity fields can then be used to advance the concentration fields over time.

Starting from the general Lagrangian equation of motion for a particle that included added mass, pressure gradient and Basset history forces, Ferry and Balachandar (2001) derived the first-order equilibrium Eulerian approximation for the particle velocity field. The accuracy of the equilibrium approximation was then tested in a turbulent channel flow by comparing the particle velocity obtained from the equilibrium approximation with the *exact* Lagrangian particle velocity. It was observed that for sufficiently small particles (with particle time scale in wall units, $\tau_+ < 1$) the equilibrium approximation provided a good approximation to the exact particle velocity and that the error in the equilibrium approximation increased slowly with increasing particle time scale.

The objective of the present work is to extend the results presented in Ferry and Balachandar (2001) and establish the applicability of the equilibrium Eulerian approximation in evolving the

particle concentration field. It is of interest to investigate if there is any systematic accumulation of error in approximating the particle velocity field with the equilibrium approach over long periods of time, in terms of the time evolution of the particle concentration field. In particular, we will evaluate the accuracy of the particle concentration field evolved over long periods of time with the equilibrium Eulerian velocity field, by comparing it with the corresponding *exact* distribution of particles evolved with the Lagrangian equations of motion. In addition to qualitative comparison of the Eulerian concentration field against the Lagrangian particle distribution, we will also present quantitative comparison of statistics on preferential concentration and gravitational settling obtained from the two approaches.

Here we choose to perform this investigating in the context of an isotropic turbulent flow in a cubic periodic box. Collisions with the wall and inter-particle collisions are two mechanisms that disturb particles away from local equilibrium. Thus by investigating the behavior of a distribution of particles at low concentration in isotropic turbulence attention is focused on examining the effectiveness of equilibrium Eulerian approximation in the absence of such collisional effects. Furthermore, unlike the turbulent channel flow, where particles continually tend to migrate towards the walls (in the absence of mechanisms such as inter-particle collision), in the case of isotropic turbulence, a statistically stationary state for the non-uniform concentration of particles can be achieved. The statistically stationary state is well suited for a thorough comparison of the equilibrium Eulerian approach with the traditional Lagrangian approach. This comparison will be made for varying particle time scale and still-fluid gravitational settling velocity.

2. Description of the simulation

2.1. Background isotropic turbulence

The unladen, forced isotropic turbulence data is obtained through direct numerical simulation, using a discrete Fourier series based pseudospectral method. The flow domain is a cubic box of length $L = 2\pi$ discretized into N^3 ($N = 96$) equispaced grid points, with periodic boundary conditions applied in all three directions. A Taylor microscale Reynolds number, Re_λ ($= u'\lambda/\nu$) $=$ 60.5, is obtained for the above grid resolution, where λ and u' are the Taylor microscale and the fluctuating rms velocity respectively.

The fluid flow is advanced by solving the governing Navier–Stokes equations in the rotational form and the continuity equation for an incompressible fluid:

$$\frac{\partial \mathbf{u}}{\partial t} + \boldsymbol{\omega} \times \mathbf{u} = -\nabla\left(\frac{p}{\rho_f} + \frac{1}{2}\mathbf{u}^2\right) + \nu\nabla^2\mathbf{u} + \mathbf{f}, \tag{1}$$

$$\nabla \cdot \mathbf{u} = 0, \tag{2}$$

where $\boldsymbol{\omega} = \nabla \times \mathbf{u}$ is the vorticity, ρ_f is the density, p the pressure, ν the kinematic viscosity of the fluid, and $\mathbf{f}$ is the external forcing applied to maintain a statistically stationary turbulence. The fluid velocity, $\mathbf{u}(\mathbf{x}, t)$, is expressed in terms of its Fourier coefficients $\hat{\mathbf{u}}$ as

$$\mathbf{u}(\mathbf{x}, t) = \sum_{\mathbf{k}} \hat{\mathbf{u}}(\mathbf{k}, t) \exp(i\mathbf{k} \cdot \mathbf{x}) \tag{3}$$

and hence,

$$\hat{\mathbf{u}}(\mathbf{k},t) = \frac{1}{N^3}\sum_{\mathbf{x}} \mathbf{u}(\mathbf{x},t)\exp(-\mathrm{i}\mathbf{k}\cdot\mathbf{x}), \tag{4}$$

where $\mathbf{k}$ and $\mathbf{x}$ represent the wavenumber and position vectors, respectively. The wavenumbers in Fourier space are given as

$$k_i = \pm n_i \frac{2\pi}{L}, \tag{5}$$

where $n_i = 0, 1, 2, \ldots, N/2$ and $i = 1, 2, 3$. The nonlinear term (the second term on the left-hand side of Eq. (1)) is advanced in time using the second-order accurate Adams–Bashforth scheme, while the linear viscous term is advanced using the second-order Crank–Nicholson method. In applying the forcing, we follow the methodology developed by Eswaran and Pope (1988a,b), where energy is added to only the largest modes in the range $0 < |\mathbf{k}| \leqslant \sqrt{8}$. In order to maintain a zero mean flow, the velocity Fourier coefficients corresponding to $\mathbf{k} = (0, 0, 0)$ are set to zero at every timestep. The unladen fluid flow field was advanced for approximately $126T_e$ before the particulate field was introduced, where T_e is the large-eddy turnover time. This time was sufficient to go past the initial transients well into the statistically stationary state for the isotropic turbulence. The timestep Δt used in the current simulations is $0.0132\tau_k$, where τ_k is the Kolmogorov timescale. The various flow parameters are listed in Table 1.

2.2. Lagrangian approach for particles

In the Lagrangian approach, the particle velocities, $\mathbf{v}$, and positions, $\mathbf{x}_p$, are obtained by solving the following equations of motion:

$$\frac{\mathrm{d}\mathbf{v}}{\mathrm{d}t} = \frac{1}{\tau_p}[\mathbf{u}(\mathbf{x}_p,t) - \mathbf{v} + \mathbf{V}_s], \tag{6}$$

$$\frac{\mathrm{d}\mathbf{x}_p}{\mathrm{d}t} = \mathbf{v}, \tag{7}$$

Table 1
Flow parameters

RMS fluctuating velocity, $\langle u'^2\rangle^{1/2}$	18.818
Energy dissipation rate, $\langle\epsilon\rangle$	3699.126
Eddy turnover time, $\langle T_e\rangle$	0.095
Taylor microscale, $\langle\lambda\rangle$	0.4462
Kolmogorov length scale, $\langle\eta\rangle$	0.02914
Kolmogorov velocity scale, $\langle v_k\rangle$	4.759
Kolmogorov time scale, $\langle\tau_k\rangle$	0.006123
Microscale Reynolds number, Re_λ	60.55
Timestep, Δt	0.00015
Wavenumber resolution factor, $k_{max}\eta$	1.36
Fluid viscosity, ν	0.1387

Properties in code units.

where the particle settling velocity in still fluid or the terminal velocity, $\mathbf{V}_s$, and the particle time scale, τ_p, are given by

$$\mathbf{V}_s = \mathbf{g}\tau_p \quad \text{and} \quad \tau_p = \frac{\rho_p d_p^2}{\rho_f 18 v}. \tag{8}$$

In the above equations, $\mathbf{g}$ is the gravity vector, d_p is the particle diameter and ρ_p is the particle density. Thus, the particle motion is taken to be in response to only the drag and gravitational forces, where again the drag force is taken to be given by the Stokes drag appropriate for small particle Reynolds numbers. In the present simulations we limit attention to only small heavier-than-fluid particles at low Reynolds numbers and hence the neglect of added-mass and Bassett history forces can be reasoned. Eqs. (6) and (7) are solved with the fourth-order Adams–Bashforth and Adams–Moulton schemes respectively. The fluid velocity at the particle location, $\mathbf{u}(\mathbf{x}_p, t)$, is computed using an optimal compact interpolation scheme.

2.3. Equilibrium Eulerian approach for the particles

In the equilibrium Eulerian approach, the particle velocity field, $\mathbf{v}(\mathbf{x}, t)$, is expressed as an expansion in terms of the fluid velocity field, given by Ferry and Balachandar (2001, 2002):

$$\mathbf{v} \approx \mathbf{v}_{eq} = \mathbf{u} + \mathbf{V}_s - \left(\frac{\mathrm{D}\mathbf{u}}{\mathrm{D}t} + \mathbf{V}_s \cdot \nabla \mathbf{u}\right)\tau_p + \mathrm{O}(\tau_p^2). \tag{9}$$

In dimensionless terms, τ_p/τ_f, the ratio of particle time scale to the characteristic time scale of the surrounding turbulent flow is the small parameter of the expansion (τ_f is the characteristic time scale of the turbulent flow, which can be chosen to be the Kolmogorov time scale). Provided the dimensionless time scale of the particle is sufficiently small, the above expansion converges rapidly and it has been shown in turbulent channel flow (Ferry and Balachandar, 2001, 2002) that even the first order ($\mathrm{O}(\tau_p)$) representation for particle velocity, as shown above in Eq. (9), provides a very good approximation to the actual Lagrangian particle velocity.

In the limit of $\tau_p \to 0$, the settling velocity of the particles vanishes (i.e., $\mathbf{V}_s \to 0$) and the particle velocity reduces to the local fluid velocity ($\mathbf{v} \to \mathbf{u}$). At small but finite τ_p, the particle velocity differs from the above limit due to two simple mechanisms. First, particles of finite inertia will not respond to local fluid acceleration ($\mathrm{D}\mathbf{u}/\mathrm{D}t$) the same way as fluid elements, resulting in a local slip velocity for the particles. Second, density difference between the particle and the fluid will result in relative settling of the particles. Furthermore, in the case of strong settling effect, where the settling velocity $\mathbf{V}_s$ is of the order of the fluctuating fluid velocity, the gravitational settling in conjunction with the fluid velocity gradient along the direction of settling introduces additional slip between the particle and the surrounding flow, owing to the memory effect of the finite inertia particles. In case of weaker gravitational effect ($\mathbf{V}_s \approx \mathbf{u}\tau_p/\tau_f$), however, the term $\mathbf{V}_s \cdot \nabla\mathbf{u}$ will be of lower order importance and can therefore be ignored to $\mathrm{O}(\tau_p)$. Nevertheless, the advantage of the above equilibrium Eulerian approximation is that it avoids the need to solve additional Navier–Stokes-like momentum (partial differential) equations for the velocity field of the particulate phase.

This velocity field, $\mathbf{v}_{\mathrm{eq}}(\mathbf{x},t)$, is used to evolve the particle concentration field. The particle concentration field, $\phi(\mathbf{x},t)$, is obtained by solving the following advection equation:

$$\frac{\partial\phi}{\partial t}+\nabla\cdot(\mathbf{v}_{\mathrm{eq}}\phi)=0. \tag{10}$$

It is well known that as the particles preferentially accumulate in regions of high strain-rate and avoid regions of high vorticity, large concentration gradients develop within the flow. Preferential concentration is most effective for particles whose time scale matches with that of the flow and for such particles the smallest spatial scale of concentration variation can be much smaller than the corresponding smallest fluid scale (the Kolmogorov length scale). Gravitational settling somewhat weakens the level of preferential concentration by decreasing the residence time of the particles within a turbulent eddy, but does not completely eliminate the tendency for preferential concentration.

A diffusion term is typically added to Eq. (10) in order to control the sharp concentration gradients and any numerical instability that may arise due to the inability to resolve such strong concentration gradients using the grid primarily chosen for computing the turbulent flow field. In the context of the present spectral simulations, recent references (Tadmor, 1989; Karamanos and Karniadakis, 2000) suggest the use of spectrally vanishing viscosity approach. In this approach a wavenumber dependent diffusion term of the form, $\epsilon\nabla\cdot[Q_{|\mathbf{k}|}\otimes\nabla\phi]$ is applied to the right-hand side of Eq. (10). In the above, ϵ is the magnitude of the numerical diffusivity, $Q_{|\mathbf{k}|}$ is the wavenumber dependent diffusivity kernel and $\otimes$ denotes the convolution operation in physical space. This additional term is a controlled diffusion term added to stabilize the numerical scheme and avoid any spurious spatial oscillations that may arise due to the inability to resolve length scales smaller than the grid resolution. However, unlike simple diffusional terms of the form, $\epsilon\nabla^2\phi$, the spectral vanishing diffusivity can be tailored to be effective only for the high wavenumber modes and to have little direct influence on the low wavenumber modes. As a consequence, in physical space, regions of sharp gradients are somewhat smoothened to grid resolution without introducing Gibb's oscillation (Canute et al., 1988; Gottlieb and Hesthaven, 2001), and the influence on the large scale variations in minimized.

As for the fluid momentum equation, the convective and diffusive terms are treated using the Adams–Bashforth (explicit) and Crank–Nicholson (implicit) schemes respectively. In Fourier space, the diffusion term is expressed as

$$\epsilon\nabla\cdot[Q_{|\mathbf{k}|}\otimes\nabla\phi]=-\epsilon\sum_{\mathbf{k}}k^2\widehat{Q}_k(t)\hat{\phi}(\mathbf{k},t)\exp(\mathrm{i}\mathbf{k}\cdot\mathbf{x}), \tag{11}$$

where $k=|\mathbf{k}|$ is the wavenumber magnitude and the hat ($\hat{}$) represents the Fourier coefficient. The viscosity kernel $\widehat{Q}_k$ is computed as follows:

$$\widehat{Q}_k=\exp\left(\frac{k^2-N^2/4}{k^2-M^2}\right),\quad 0<M^2<k^2\leqslant N^2/4, \tag{12}$$

$$\widehat{Q}_k=0,\quad 0\leqslant k^2\leqslant M^2, \tag{13}$$

$$\widehat{Q}_k=1,\quad k^2>N^2/4, \tag{14}$$

where M is the cutoff wavenumber magnitude below which the diffusive term has no effect. In the present computations, $M = 6$ is chosen, based on the recommendation in Tadmor (1989) and Karamanos and Karniadakis (2000). However, note that the kernel becomes O(1) only for large k. For example, in the present problem the kernel is less than 4% for all $k \leqslant N/4$. In the absence of numerical diffusion, there is a constant build up of "energy" at the high wavenumbers in the power spectrum of the particle concentration, primarily due to the aliasing error. The introduction of the spectral vanishing viscosity will prevent the unphysical accumulation of energy at the highest resolved wavenumbers and can be thought of as a strategy for dealiasing. The viscosity coefficient, ϵ, is chosen such that it is sufficiently large to damp spurious high wavenumber oscillations, yet small enough not to significantly affect the concentration field at the large and intermediate scales of importance. Based on Karamanos and Karniadakis (2000), ϵ is computed as follows:

$$\epsilon = \frac{c}{N}, \tag{15}$$

where c is a constant and N ($=96$) is the number of grid points in any one direction. Diagnostic tests were performed to choose a suitable value for c. Values varying over four orders of magnitude ranging from 0.1 to 1000 were considered. It was observed that $c < 50$ could lead to oscillations in the values of particle concentration. Hence, a value of $c = 75$ was chosen. Further discussion regarding the effects of ϵ on the Eulerian statistics is provided in the results section. As pointed out in Tadmor (1989) and Karamanos and Karniadakis (2000), the above approach provides an essentially non-oscillatory behavior for the solution and also maintains the spectral accuracy.

3. Results

3.1. Equilibrium Eulerian particle velocity

First, we will address the accuracy of the equilibrium expansion given in Eq. (9) in approximating the *exact* instantaneous velocity of the particle, in the context of isotropic turbulence. Here, the *exact* particle velocity is defined to be that obtained from Lagrangian tracking using Eqs. (6) and (7) and the error in the first-order equilibrium approximation, E_1 is then defined as

$$E_1 = \left[\frac{1}{N_\mathrm{p}}\sum_{i=1}^{N_\mathrm{p}}(\mathbf{v}_i - \mathbf{v}_{\mathrm{eq},i})^2\right]^{1/2} \quad \text{and} \quad E_0 = \left[\frac{1}{N_\mathrm{p}}\sum_{i=1}^{N_\mathrm{p}}(\mathbf{v}_i - \mathbf{u}(\mathbf{x}_{\mathrm{p}i}))^2\right]^{1/2}, \tag{16}$$

where the sum is over all the N_p particles inside the isotropic box of turbulence, with the position vector of the ith particle given by $\mathbf{x}_{\mathrm{p}i}$, $\mathbf{v}_i$ is the *exact* velocity of the ith particle and $\mathbf{v}_{\mathrm{eq},i}$ represents the velocity of ith particle evolved using the equilibrium Eulerian velocity field. The error in the first-order approximation can also be compared with that of the zeroth order approximation, E_0, where the particle velocity is approximated simply as the local fluid velocity interpolated to the particle position. Fig. 1 shows the above root mean square errors plotted as a function of nondimensional particle time scale. All the quantities are made dimensionless by the fluid

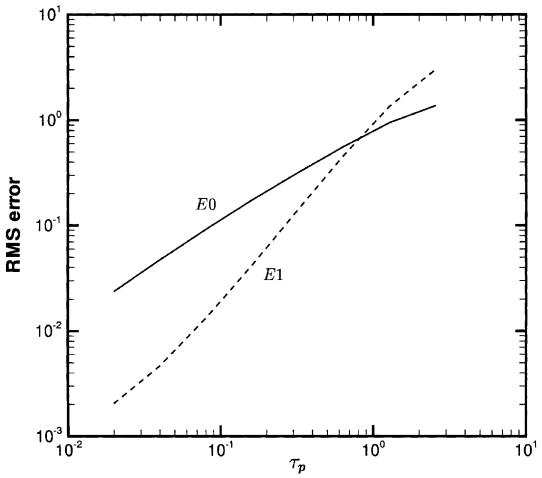

Fig. 1. Comparison of rms zeroth and first order errors for dense particles.

Kolmogorov length, velocity and time scales. It is clear that for small particles of $\tau_p < 1$, the first-order equilibrium expansion provides a better approximation to the actual particle velocity and with decreasing particle size, the error decreases more rapidly when the $O(\tau_p)$ correction is applied to the equilibrium particle velocity, as given in Eq. (9).

In the work by Ferry and Balachandar (2001), it was pointed out in the context of a turbulent channel flow that the equilibrium approximation accurately captures important physics such as preferential accumulation and turbophoretic migration for sufficiently small particles. Here, we observe similar behavior in the context of isotropic turbulence as well. Only sample result for the statistics of $(|\mathbf{S}|^2 - |\mathbf{\Omega}|^2)$ is presented here. It has been well established by Maxey (1987) that $(|\mathbf{S}|^2 - |\mathbf{\Omega}|^2)$ provides a simple quantitative measure of preferential accumulation, as can be shown from Eq. (9) that

$$\nabla \cdot \mathbf{v} = -\tau_p \frac{\partial u_i}{\partial x_j} \frac{\partial u_j}{\partial x_i} = -\tau_p (|\mathbf{S}|^2 - |\mathbf{\Omega}|^2), \tag{17}$$

where $\mathbf{S}$ and $\mathbf{\Omega}$ are the symmetric (strain-rate) and antisymmetric (rotation-rate) parts of the fluid velocity gradient. Here, we evolve two sets of Lagrangian particles. The first set is the *exact* set of particles evolved using the equations of motion (Eqs. (6) and (7)), while the second *approximate* set of Lagrangian particles is evolved over time using Eq. (7) with the instantaneous particle velocity given by the local equilibrium Eulerian velocity field interpolated to the particle location. The degree of preferential concentration captured by the two sets of particles is measured in terms of the mean value, $\langle |\mathbf{S}|^2 - |\mathbf{\Omega}|^2 \rangle_p$, where the angle brackets indicate an average over all the particle locations (see Eq. (18) for the definition) and the overbar indicates a time-average. Fig. 2 presents $\langle |\mathbf{S}|^2 - |\mathbf{\Omega}|^2 \rangle_p$ averaged over both the *exact* and *approximate* particles for varying τ_p. For comparison, it should be pointed out that $(|\mathbf{S}|^2 - |\mathbf{\Omega}|^2)$ averaged over the entire fluid volume is zero. In other words, if an initial uniform distribution of particles were to be evolved with the simple approximation $\mathbf{v} \approx \mathbf{u}$, then there will be no preferential concentration and $\langle |\mathbf{S}|^2 - |\mathbf{\Omega}|^2 \rangle_p = 0$. Thus, the positive value for $\langle |\mathbf{S}|^2 - |\mathbf{\Omega}|^2 \rangle_p$ indicates that particles of finite inertia prefer regions

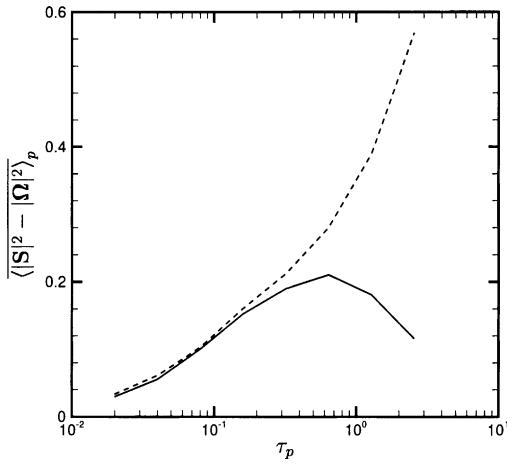

Fig. 2. Variation of $\overline{\langle |\mathbf{S}|^2 - |\mathbf{\Omega}|^2 \rangle_p}$ with τ_p for particles. Lagrangian (—); equilibrium Eulerian (- - -).

where strain-rate is in excess of rotation-rate. This preferential concentration is well captured by the equilibrium approximation for particles of $\tau_p < 0.2$. For larger particles the departure from the exact behavior increases, with the equilibrium approximation tending to overpredict the degree of preferential accumulation.

Fig. 3 presents the probability density function (PDF) of $(|\mathbf{S}|^2 - |\mathbf{\Omega}|^2)$ obtained from both the *exact* and *approximate* sets of particles. Also plotted for comparison is the corresponding PDF for the fluid. The results are shown for the case of $\tau_p = 0.64$ particles, for which in Fig. 2 the equilibrium approximation was observed to be different from the exact statistics. Fig. 3 shows that the PDF of the inertial particles is significantly different from that of the fluid. Compared to this difference, the difference in the PDFs of the *exact* and *approximate* particles is much smaller. Thus

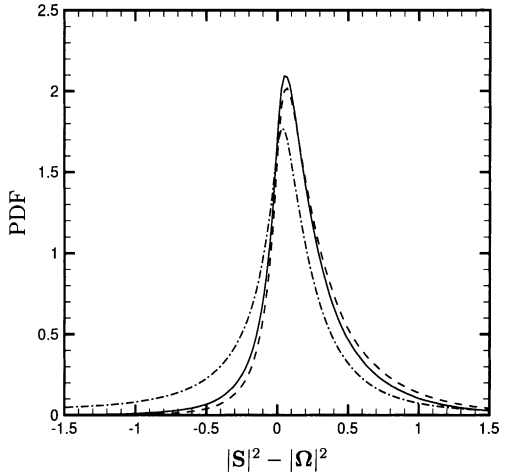

Fig. 3. Comparison of PDFs of $|\mathbf{S}|^2 - |\mathbf{\Omega}|^2$ for $\tau_p = 0.64$ particles. Lagrangian (—); equilibrium Eulerian (- - -); fluid (–·–·–).

it appears that even for larger particles of $\tau_p \approx 1$ the equilibrium approach continues to offer better approximation to particle velocity than $\mathbf{v} \approx \mathbf{u}$.

3.2. Equilibrium Eulerian concentration

In this section, we will go beyond the Lagrangian tracking of particles with the equilibrium approximation and evolve a particle concentration field with the equilibrium Eulerian particle velocity field. By comparing the Eulerian concentration field with the *exact* Lagrangian distribution of particles, we will assess the feasibility and accuracy of the equilibrium Eulerian approach for long-time evolution of particle concentration field. In the current work, 12 cases involving variation of dimensionless particle response time, τ_p, and the dimensionless still-fluid settling (or terminal) velocity, $\mathbf{V}_s$, are considered. Four values of response time, $\tau_p = 0.05, 0.1, 0.2, 0.4$, and three values of settling velocity, $|\mathbf{V}_s| = 0.5, 2, 4$ are chosen. The number of Lagrangian particles considered is 48^3, which are initially located at the positions of alternate grid points. The initial velocities of the Lagrangian particles are equal to the equilibrium Eulerian velocities interpolated to their locations. The influence of initial location and velocity of the particles are forgotten quickly over a few dimensionless time scales of the particle. Along with the Lagrangian particles, the Eulerian concentration field is also evolved using the equilibrium Eulerian velocity for all the 12 cases independently. The initial concentration field is taken to be uniform and in all cases considered, the concentration field quickly reaches a statistically stationary state. The smaller particles corresponding to $\tau_p = 0.05$ are evolved for 4000 response times, whereas the largest ones ($\tau_p = 0.4$) are evolved for 500 response times. These evolution times are sufficient for both the Eulerian and Lagrangian statistics to reach a statistically stationary state.

The primary purpose of the present paper is to evaluate the fidelity of the Eulerian approach for the particle concentration field, evolved with the equilibrium Eulerian particle velocity field, by comparing it with the corresponding Lagrangian distribution of particles, which serves as the benchmark. Fig. 4 presents a comparison between the Lagrangian and the equilibrium Eulerian results for the case of $\tau_p = 0.1$ and $\mathbf{V}_s = 4$. Frame (b) shows the contours of Eulerian particle concentration field on a vertical plane passing through the cubic box of isotropic turbulence at one instant in time and frame (c) shows the corresponding Lagrangian distribution of particles on a thin slice of volume surrounding this plane. A satisfactory qualitative agreement between the two frames can be observed, with both showing a non-uniform concentration of particles with preferential accumulation in selected regions of the flow and certain other locations void of any particles. In Fig. 4, frame (a) shows contours of $(|\mathbf{S}|^2 - |\mathbf{\Omega}|^2)$ on the same vertical plane as in frame (b). The comparison between the Eulerian particle concentration field and the contours of $(|\mathbf{S}|^2 - |\mathbf{\Omega}|^2)$ is quite striking. It is clear particles accumulate in regions where strain-rate dominates over local vorticity and avoid local regions where the rotation-rate is much in excess of the local strain-rate.

In spite of the qualitative agreement between the three frames shown in Fig. 4, a quantitative comparison of the Eulerian concentration field with the Lagrangian distribution of particles can be challenging. For example, it is not straight forward to obtain a statistically accurate concentration field from the Lagrangian distribution of particles for comparison with the corresponding Eulerian result. Here, we propose to compute the statistics of different fluid and particle quantities as seen by both the distribution of Lagrangian particles and by the Eulerian particle concentration

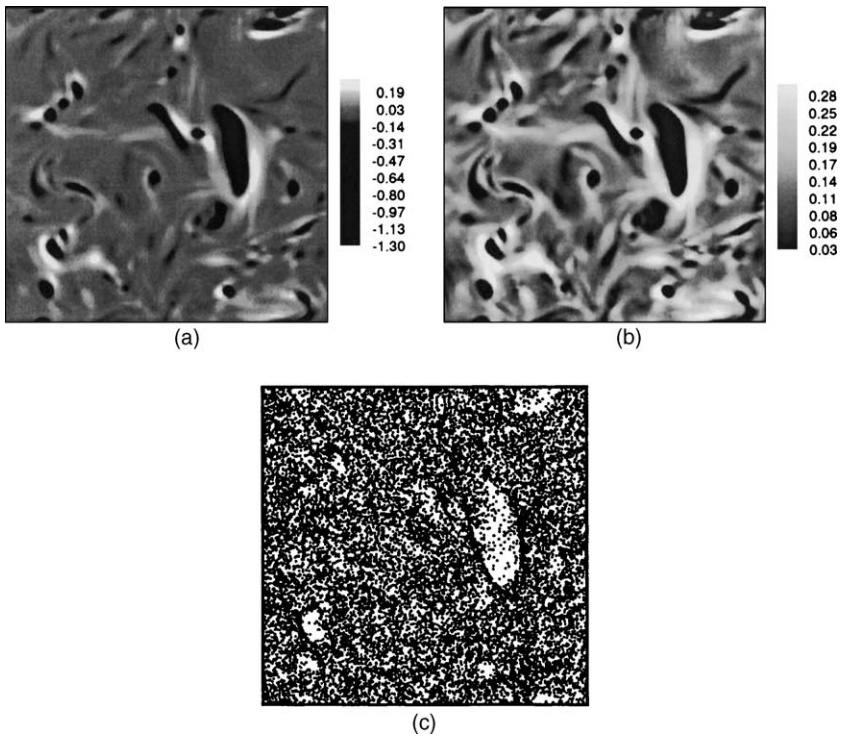

Fig. 4. Contours of (a) $|\mathbf{S}|^2 - |\mathbf{\Omega}|^2$, (b) $\phi(\mathbf{x}, t)$ and (c) particle position scatter, for $\tau_p = 0.1$ and $\mathbf{V}_s = 4$.

field and compare them to assess the accuracy of the equilibrium Eulerian approach. All statistics to be presented below are for quantities that have been non-dimensionalized by the corresponding Kolmogorov scale.

The particle-average of a quantity f seen by the distribution of Lagrangian particles can be defined as follows:

$$\text{Lagrangian}: \quad \langle f \rangle_p(t) = \frac{1}{N_p} \sum_{i=1}^{N_p} f_i(\mathbf{x}_{pi}, t) \tag{18}$$

and the corresponding particle-average seen by the Eulerian particle concentration can be evaluated as:

$$\text{Eulerian}: \quad \langle f \rangle_p(t) = \frac{\sum_{i=1}^{N_x} \sum_{j=1}^{N_y} \sum_{k=1}^{N_z} \phi(x_i, y_j, z_k, t) f(x_i, y_j, z_k, t)}{\sum_{i=1}^{N_x} \sum_{j=1}^{N_y} \sum_{k=1}^{N_z} \phi(x_i, y_j, z_k, t)}. \tag{19}$$

In the above equations, $N_x N_y N_z$ is the total number of grid points (96^3 in this case) and x_i, y_j, z_k represent the grid point coordinates in the physical space. As can be observed, the Eulerian statistics are weighted by the local particle concentration.

We also define a simple spatial average taken over the entire box of isotropic turbulence, denoted by $\langle \cdot \rangle$. The volume-averaged mean Eulerian concentration of particles, $\langle \phi \rangle$, remains time-invariant and the spectral vanishing viscosity has no effect on the mean conservation of mass. The

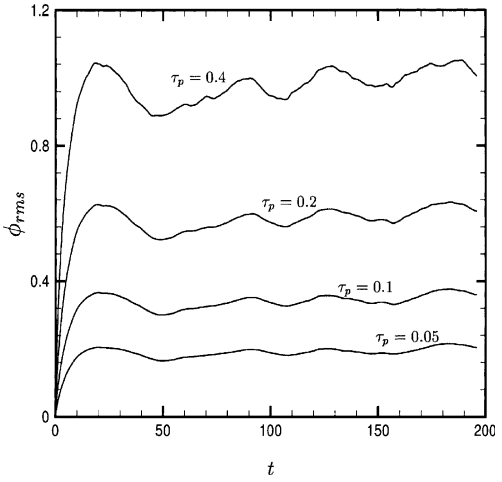

Fig. 5. Normalized rms particle concentration, ϕ_{rms}, for $|\mathbf{V}_{\mathrm{s}}| = 2$. Time t is normalized with the Kolmogorov timescale.

time history of the root mean square fluctuation in particle concentration for the four different particles of $\tau_{\mathrm{p}} = 0.05, 0.1, 0.2$ and 0.4 at the intermediate settling velocity $|\mathbf{V}_{\mathrm{s}}| = 2$ is shown in Fig. 5. The figure shows the normalized rms concentration fluctuation, ϕ_{rms}, defined as

$$\phi_{\mathrm{rms}} = \frac{\langle (\phi - \langle \phi \rangle)^2 \rangle^{1/2}}{\langle \phi \rangle}. \tag{20}$$

After a short period of initial transience, where ϕ_{rms} rapidly increases from its initial value of zero, it reaches a statistically steady state in all the cases considered. Time-averaged value of ϕ_{rms}, averaged only over the period of statistical stationarity, is presented in Table 2 for all the cases

Table 2
Comparison of the computed skewness with the log-normal values for various τ_{p} and $|\mathbf{V}_{\mathrm{s}}|$

$\lvert\mathbf{V}_{\mathrm{s}}\rvert$	τ_{p}	ϕ_{rms}, current	Skewness, S_ϕ	
			Current	Log-normal
0.5	0.05	0.2222	−1.4035	0.6784
	0.10	0.3886	−0.6985	1.2258
	0.20	0.6422	0.0724	2.1933
	0.40	1.0215	0.9909	4.1343
2.0	0.05	0.1943	−1.3560	0.5910
	0.10	0.3464	−0.6515	1.0817
	0.20	0.5922	0.1464	1.9886
	0.40	0.9927	1.1425	3.9601
4.0	0.05	0.1594	−1.1809	0.4829
	0.10	0.2934	−0.5358	0.9064
	0.20	0.5259	0.2420	1.7253
	0.40	0.9359	1.2952	3.6326

considered. Here the overbar represents a time-average. The level of fluctuation in particle concentration increases with particle response time, reaching as large as the mean for the largest particle considered. With increasing settling velocity the residence time of particles within the turbulent eddies decreases and as a result $\overline{\phi_{\mathrm{rms}}}$ decreases with increasing $\mathbf{V}_{\mathrm{s}}$. For the larger particles under consideration the decrease is only modest as $|\mathbf{V}_{\mathrm{s}}|$ increases from 0.5 to 4.0. Table 2 also presents the time-averaged skewness of particle concentration defined as

$$S_{\phi} = \overline{\left[\frac{\langle (\phi - \langle \phi \rangle)^3 \rangle}{\langle (\phi - \langle \phi \rangle)^2 \rangle^{3/2}} \right]} \tag{21}$$

for the 12 different cases. Log-normal distribution is an appropriate reference to compare the actual distribution of concentration. The skewness factor for the log-normal distribution is defined as

$$S_{\mathrm{LN}} = \overline{\phi_{\mathrm{rms}}}[(\overline{\phi_{\mathrm{rms}}})^2 + 3]. \tag{22}$$

Thus, from Table 2, it appears that the distribution of particle concentration differs from log-normal. Interestingly, the skewness is negative for small particle time scale, which arises mainly because the positive fluctuations are somewhat contained than the negative fluctuations about the mean, which is illustrated in Fig. 6, where the PDF of the deviation in particle concentration away from the mean $(\phi - \langle \phi \rangle)$ is plotted for the $\tau_{\mathrm{p}} = 0.05$ particle. The peak concentration within the box was observed to quickly reach a statistically stationary state. Although the precise value of peak concentration fluctuates over time, for the all the three cases shown in Fig. 6, it varies between 150% and 190% of the mean concentration. With increasing particle time scale, the distribution of particle concentration widens and consequently the skewness becomes positive and increases, but for all cases considered it remains smaller than that of log-normal distribution.

The effect of spectral vanishing diffusivity on the computed concentration field can be best illustrated with the energy spectra of concentration. In Fig. 7, $|\hat{\phi}|^2$ is plotted against $|\mathbf{k}|$ for five

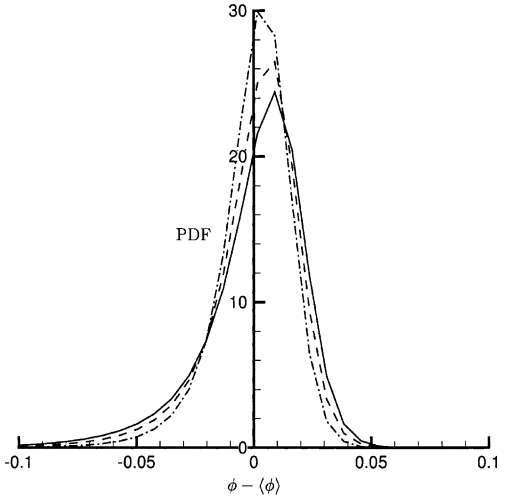

Fig. 6. Fluctuating particle concentration PDFs for $\tau_{\mathrm{p}} = 0.05$. $|\mathbf{V}_{\mathrm{s}}| = 0.5$ (—); $|\mathbf{V}_{\mathrm{s}}| = 2$ (- - -); $|\mathbf{V}_{\mathrm{s}}| = 4$ (–·–·–).

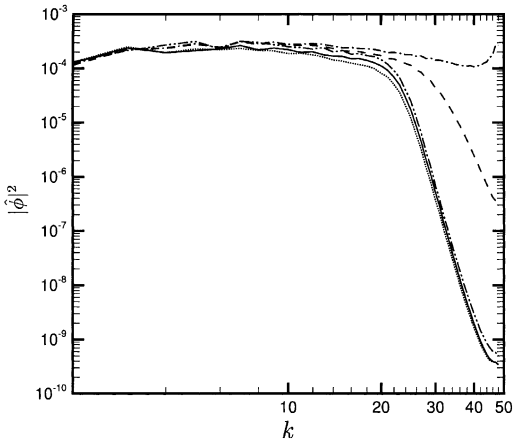

Fig. 7. Particle concentration power spectrum for various values of diffusivity coefficient and $\tau_p = 0.1$ and $\mathbf{V}_s = 4$. $\epsilon = 1000/N$ (···); $\epsilon = 100/N$ (—); $\epsilon = 75/N$ (–··–··–); $\epsilon = 10/N$ (- - -); $\epsilon = 1/N$(–·–·–).

different values of $\epsilon = 1/N, 10/N, 75/N, 100/N$ and $1000/N$, covering three orders of magnitude. Even though the velocity field is well resolved and shows several decades of energy decay, the corresponding spectra of the concentration field for small values of ϵ (i.e., without much spectral vanishing diffusivity) do not show any spectral decay and exhibit spurious build up of energy at the high wavenumbers. Without any diffusivity, sharp gradients are inevitable in the solution of Eq. (10) and the inability to resolve such sharp gradients in concentration results in the spectral build up at the highest wavenumbers. With the introduction of spectral vanishing viscosity of reasonable magnitude, the high wavenumber part of the concentration spectra is dramatically smoothened. This in physical space corresponds to a dramatic reduction in the high frequency spatial oscillations that otherwise will appear in regions of strong concentration gradient due to Gibb's phenomenon (Canute et al., 1988). This behavior is consistent with the observations by Tadmor (1989) and Karamanos and Karniadakis (2000). Such large oscillations in the present context can result in local regions of negative concentration. The spectral vanishing viscosity greatly reduces the magnitude and the extent of these negative concentrations. The influence of spectral vanishing viscosity is relatively small for the low wavenumber range, but increases with increasing ϵ. The choice of $\epsilon = 75/N$ chosen here is a compromise, where the high wavenumber spurious oscillations are damped and the effect on large scale concentration variation is minimized.

Fig. 8 presents the temporal evolution of the following particle-averaged statistics: $\langle |\mathbf{S}|^2 - |\mathbf{\Omega}|^2 \rangle_p$, $\langle |\mathbf{S}| \rangle_p$, $\langle |\mathbf{\Omega}| \rangle_p$, and $\langle |\sigma_u| \rangle_p$, computed based on both the Lagrangian particle distribution and the equilibrium Eulerian concentration field. Here, σ_u is the largest negative (most compressional) eigenvalue of the strain-rate tensor, $\mathbf{S}$. The results shown are for $\tau_p = 0.1$ and $|\mathbf{V}_s| = 4$. These particles are evolved for 2000 response times and as can be seen, after an initial period of transience, the statistics attain a stationary state. From Eq. (17), it can be seen that $(|\mathbf{S}|^2 - |\mathbf{\Omega}|^2)$, averaged over the entire box of turbulence, is constrained to be zero. For the fluid as a whole, thus, mean square strain-rate is in exact balance with the mean square rotation-rate. Fig. 8(a) shows that $\langle |\mathbf{S}|^2 - |\mathbf{\Omega}|^2 \rangle_p$ averaged over the particles, however, becomes positive and in the

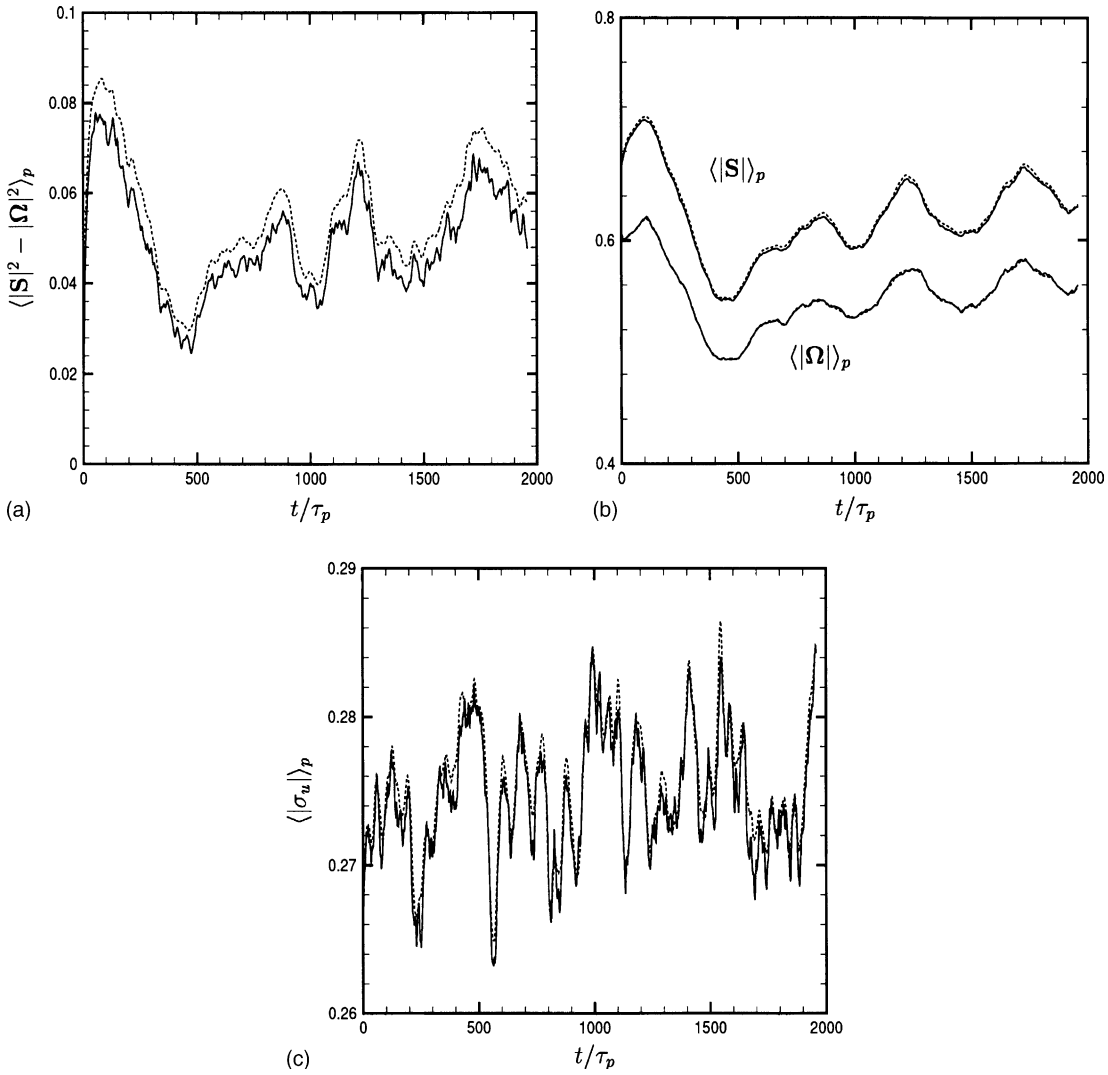

Fig. 8. Time variation of (a) $\langle |\mathbf{S}|^2 - |\mathbf{\Omega}|^2 \rangle_p$, (b) $\langle |\mathbf{S}| \rangle_p$ and $\langle |\mathbf{\Omega}| \rangle_p$ (c) $\langle |\sigma_u| \rangle_p$, for $\tau_p = 0.1$ and $|\mathbf{V}_s| = 4$. Lagrangian (—); equilibrium Eulerian (- - -).

statistically stationary state, fluctuates about a value of approximately 0.05. Thus the particles tend to preferentially accumulate in regions where local strain-rate is in excess of local rotation-rate. The $\tau_p = 0.1$ particles are sufficiently small that the time evolution of the statistics based on equilibrium Eulerian particle concentration is in good agreement with that based on the "true" Lagrangian distribution of particles. The equilibrium Eulerian concentration slightly overpredicts the degree of preferential accumulation, which is consistent with the result presented in Fig. 2. It must however be remarked that these particles are not so small that they follow the fluid entirely. This is reflected by the degree of preferential accumulation observed for these particles, which has been captured by the equilibrium Eulerian approach as accurately as in the Lagrangian tracking of particles.

The good agreement between the equilibrium Eulerian and Lagrangian approaches can also be seen in the time evolution of $\langle|\mathbf{S}|\rangle_p$ and $\langle|\mathbf{\Omega}|\rangle_p$. The strain-rate and rotation-rate magnitudes averaged over the entire volume of fluid, ($\langle|\mathbf{S}|\rangle$ and $\langle|\mathbf{\Omega}|\rangle$), are respectively 0.6805 and 0.6289. Note that although $\langle|\mathbf{S}|^2\rangle = \langle|\mathbf{\Omega}|^2\rangle$, since large values of rotation rate are more likely to occur than strain-rate, we have the statistical result $\langle|\mathbf{S}|\rangle > \langle|\mathbf{\Omega}|\rangle$. From Fig. 8(b), it can be seen that both the strain-rate and rotation-rate averaged over the particles are less than the corresponding fluid average. Particles are clearly expected to avoid regions of high rotation-rate, but they also seem not to prefer regions of high strain-rate. This behavior that particle concentration tends to diminish in regions of very high strain-rate has previously been observed by Wang and Maxey (1993) as well. They suggest that this may be due to the fact that the regions of high strain-rate often surround the intense vortex tubes and thus particles may be spun out of these intense strain-rate regions as well.

Also shown in Fig. 8 is the time history of $\langle|\sigma_u|\rangle_p$. The significance of this quantity is that in Ferry and Balachandar (2001) it was shown that $1/|\sigma_u|$ provides the appropriate time scale of the fluid flow and that provided $\tau_p|\sigma_u| \leqslant 1$ over the entire volume, an Eulerian representation for the particle velocity is meaningful. If the above condition is satisfied, any deviation in the particle velocity will decay exponentially fast and entrain to the unique Eulerian velocity, whereas for $\tau_p|\sigma_u|$ much greater than 1, an Eulerian description for particle velocity is appropriate only in a local average sense. It is clear from Fig. 8(c) that, on average, the assumption of $\tau_p|\sigma_u| \leqslant 1$ is well satisfied by the $\tau_p = 0.1$ particles. In fact, even for the largest particles of $\tau_p = 0.4$ under consideration, the assumption of a unique Eulerian velocity field is appropriate. As in the case of strain-rate and rotation-rate results, the Lagrangian and equilibrium Eulerian statistics compare quite well.

It is now well established that particles falling through isotropic turbulence do not sample the flow uniformly. Particles prefer to flow down regions of downwash than move down through regions of upwash. As a result, the mean vertical fluid velocity seen by the particles is non-zero and is pointed down, even though the mean fluid velocity of the box of isotropic turbulence is zero. Thus, the settling velocity of particles in isotropic turbulence is higher than its value in still fluid (Wang and Maxey, 1993). Fig. 9(a) and (b) shows the time history of the mean vertical velocity of the fluid seen by the particles and that of the particles, $\langle u_1\rangle_p$ and $\langle v_1\rangle_p$, evaluated with both the Lagrangian and equilibrium Eulerian approaches for the case of $\tau_p = 0.1$ and $|\mathbf{V}_s| = 4.0$. It is clear that as in the Lagrangian approach, the equilibrium Eulerian approximation also accurately captures the increase in settling velocity. For the case of $\tau_p = 0.1$ and $|\mathbf{V}_s| = 4.0$, the settling velocity on average increases by about 0.15, which is precisely the mean local vertical fluid velocity seen by the particles. Shown in Fig. 9(c) and (d) are the rms fluctuations in the vertical and horizontal components of particle velocity defined as

$$v_{1,\mathrm{rms}} = \langle(v_1 - \langle v_1\rangle)^2\rangle_p^{1/2} \quad \text{and} \quad v_{2,\mathrm{rms}} = \langle v_2^2\rangle_p^{1/2}. \tag{23}$$

The agreement between the Lagrangian and the equilibrium Eulerian statistics is quite good. It can also be observed that the Eulerian approach compares better with the Lagrangian results with respect to the low frequency oscillations than the high frequency ones.

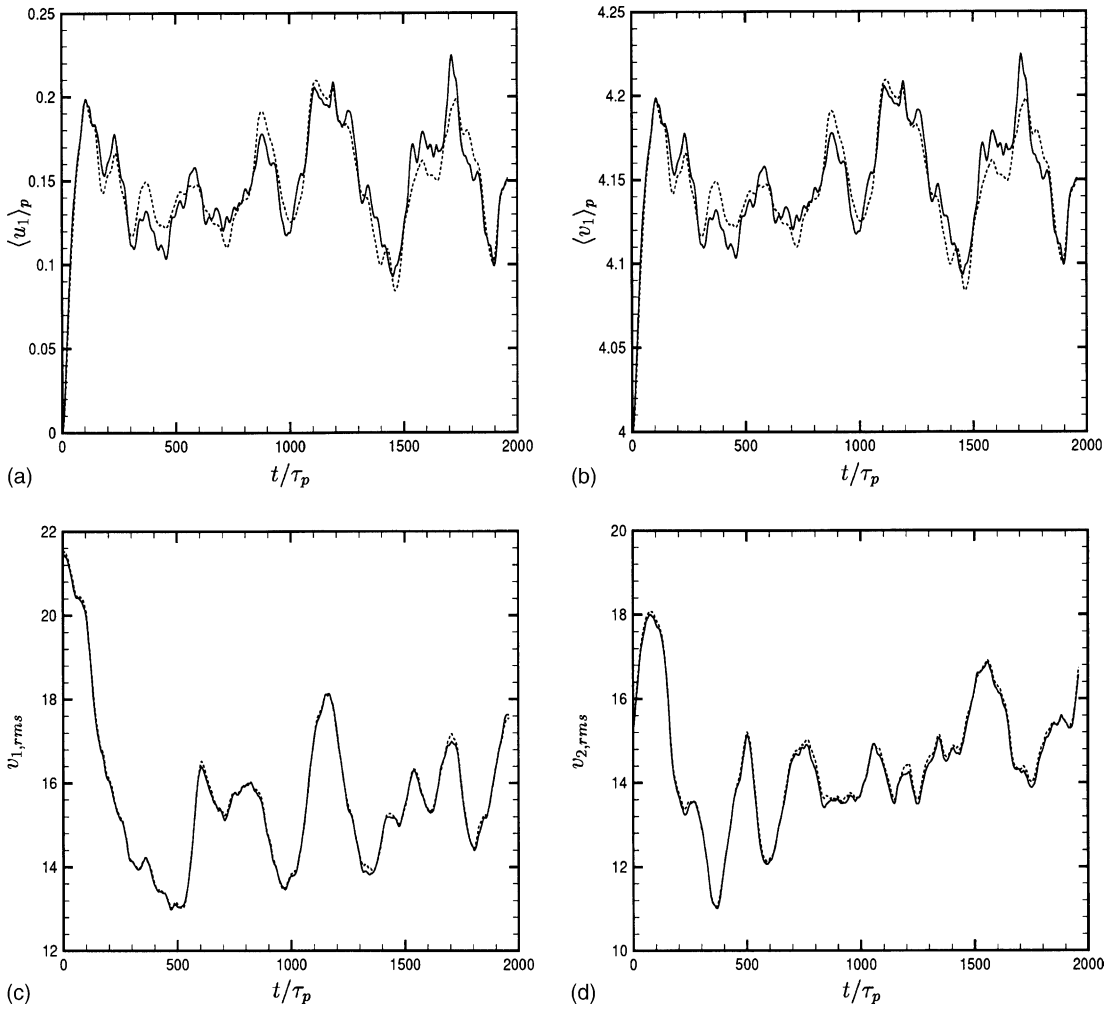

Fig. 9. Time variation of (a) $\langle u_1 \rangle_p$, (b) $\langle v_1 \rangle_p$, (c) $v_{1,rms}$, (d) $v_{2,rms}$, for $\tau_p = 0.1$ and $|\mathbf{V}_s| = 4$. Lagrangian (—); equilibrium Eulerian (- - -).

3.3. Effects of gravity and particle response time

In the previous section, we focused attention mainly on the particle-averaged statistics of only a single particle class characterized by $\tau_p = 0.1$ and $|\mathbf{V}_s| = 4.0$. The time-dependent behavior of all other particle classes was qualitatively quite similar and in particular, a statistically stationary state was obtained after an initial transience in all cases. The level of accuracy of the equilibrium Eulerian approximation, however, depends on the particle response time and the gravitational settling. Here we present statistics that are further averaged over time in the statistically stationary regime. These time- and particle-averaged statistics are presented as a function of the particle response time, τ_p, and the particle still-fluid settling velocity, $|\mathbf{V}_s|$.

Fig. 10(a) shows the variation in $\overline{\langle|\mathbf{S}|\rangle_p}$ and $\overline{\langle|\mathbf{\Omega}|\rangle_p}$ for the 12 cases, obtained from both the Lagrangian and the equilibrium Eulerian approaches. First, it can be observed that with increasing τ_p, $\overline{\langle|\mathbf{S}|\rangle_p}$ increases far more slowly than the steady and rapid decrease in $\overline{\langle|\mathbf{\Omega}|\rangle_p}$. This suggests that the particles of increasing inertia tend to avoid regions of high vorticity far more effectively than they tend to seek regions of high strain-rate. The rotation-rate statistic shows an interesting behavior. For particles of smaller inertia, $\overline{\langle|\mathbf{\Omega}|\rangle_p}$ obtained from the Lagrangian approach is lower than the corresponding Eulerian estimate. With increasing τ_p, a crossover takes place and then the Eulerian estimate tends to be lower than the corresponding Lagrangian statistics.

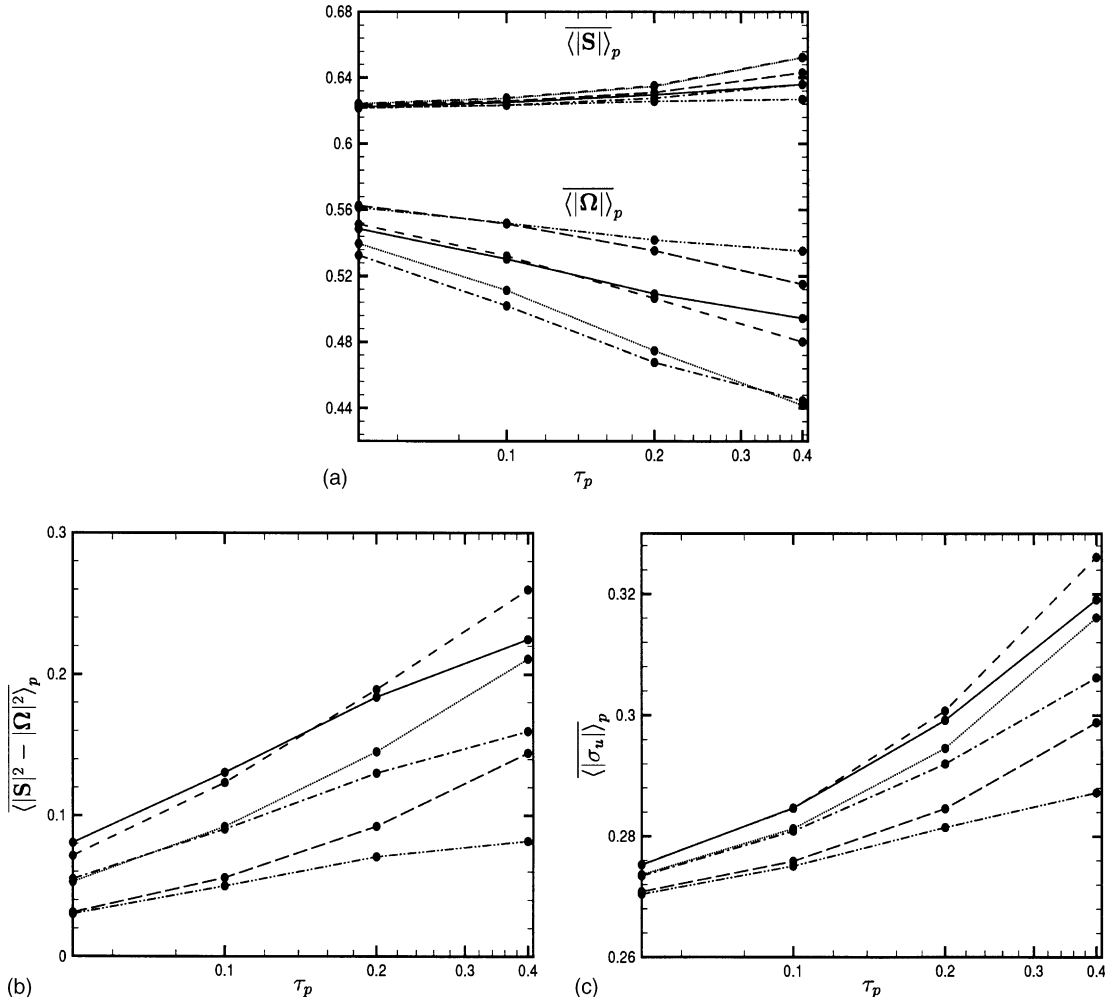

Fig. 10. Variation of (a) $\overline{\langle|\mathbf{S}|\rangle_p}$ and $\overline{\langle|\mathbf{\Omega}|\rangle_p}$, (b) $\overline{\langle|\mathbf{S}|^2 - |\Omega|^2\rangle_p}$, (c) $\overline{\langle|\sigma_u|\rangle_p}$, with $\mathbf{V}_s$ and τ_p. Lagrangian (—) and equilibrium Eulerian (- - -) for $\mathbf{V}_s = 0.5$; Lagrangian (– · – · –) and equilibrium Eulerian (· · ·) for $\mathbf{V}_s = 2$; Lagrangian (– ·· – ·· –) and equilibrium Eulerian (- - -) for $\mathbf{V}_s = 4$.

The above behavior is due to two competing mechanisms. First, as seen in Fig. 2, the $O(\tau_p)$ equilibrium Eulerian approximation for particle velocity given in Eq. (9) tends to overpredict the preferential accumulation. This effect is negligible for particles of small inertia, but slowly increases as τ_p increases. The second effect is due to the spectral vanishing viscosity employed in the Eulerian approach, which tends to smoothen and somewhat broaden the sharp gradients. The net effect of this diffusion is to counter the effect of preferential accumulation and increase the Eulerian estimate of $\overline{\langle|\mathbf{\Omega}|\rangle_p}$. This effect is dependent on the degree of preferential accumulation and therefore can be expected to peak when the time scale of the particle matches with that of the turbulence. Furthermore, with increasing settling, preferential accumulation and particle concentration gradients weaken and correspondingly the diffusion effect weakens as well. In the limit of small τ_p, the latter effect dominates and as a result, the Lagrangian particles tend to avoid regions of rotation-rate more effectively than the Eulerian particle concentration, whereas as τ_p increases, the former effect takes over and the equilibrium approximation underpredicts $\overline{\langle|\mathbf{\Omega}|\rangle_p}$.

The above two mechanisms influence the strain-rate statistics as well. However, as pointed above, the degree of attraction towards the high strain-rate regions is not nearly as high as the abhorrence towards the high rotation-rate regions and as a result the concentration gradient associated with the high strain-rate regions is weaker than that in regions of strong rotation. In effect, the diffusion effect is weaker in case of strain-rate statistics. Therefore, for all cases considered, the equilibrium Eulerian approach estimates a slightly $\overline{\langle|\mathbf{S}|\rangle_p}$ compared to the Lagrangian statistics and the difference increases with increasing particle time scale. Nevertheless, in all the cases considered here, the equilibrium Eulerian approach provides a reasonable approximation to the actual Lagrangian tracking of particles.

The statistics on preferential concentration measured in terms of $\overline{\langle|\mathbf{S}|^2-|\mathbf{\Omega}|^2\rangle_p}$ for both the Lagrangian and Eulerian approaches are shown in Fig. 10(b). Increasing tendency towards preferential accumulation with increasing τ_p is evident. On the other hand, gravitational settling tends to homogenize the distribution of particles. The difference between the equilibrium Eulerian and the Lagrangian approaches generally increases with the particle response time. However, for the case of $|\mathbf{V}_s| = 0.5$, the effect of crossover seen earlier in the rotation-rate statistics can be observed. The variation in $\overline{\langle|\sigma_u|\rangle_p}$ is shown in Fig. 10(c). In all the cases considered, the equilibrium Eulerian approximation predicts a somewhat larger value than the Lagrangian estimate. The difference is negligible for particles of small time scale, but it increases with increasing τ_p.

The PDF of $|\mathbf{S}|$ measured at the particle locations obtained from both the Lagrangian and equilibrium Eulerian approaches are shown in Fig. 11. The results for two different types of particles are shown: (1) $\tau_p = 0.1$, $|\mathbf{V}_s| = 4.0$, whose time evolution was shown in Fig. 8(b); and (2) $\tau_p = 0.4$, $|\mathbf{V}_s| = 0.5$, which shows the worst case difference between the Eulerian and Lagrangian approaches. The entire cubic box of data over a period of time after statistical stationarity has been achieved is used to compute these PDFs. Also shown are the corresponding fluid PDFs computed for the entire fluid volume. Owing to preferential accumulation, the particle PDFs are different from the corresponding fluid PDF and the difference increases with increasing τ_p. Compared to this difference, the discrepancy between the Lagrangian and equilibrium Eulerian PDFs is not as large, even for the worst case. For the case of $\tau_p = 0.1$ and $|\mathbf{V}_s| = 4.0$, the Lagrangian and the equilibrium Eulerian PDFs virtually overlap. The corresponding PDFs of $|\mathbf{\Omega}|$ are shown in Fig. 12(a) and (b) and the conclusions are the same, i.e. even for the case of $\tau_p = 0.4$,

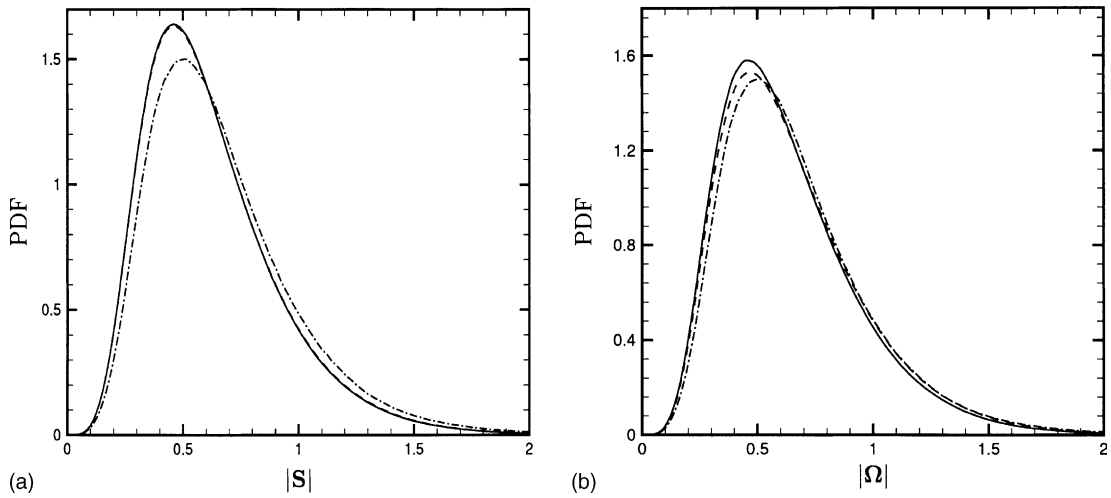

Fig. 11. Temporally and spatially averaged PDFs of $|\mathbf{S}|$ for (a) $\tau_p = 0.1$ and $|\mathbf{V}_s| = 4$, (b) $\tau_p = 0.4$ and $|\mathbf{V}_s| = 0.5$. Lagrangian (—); equilibrium Eulerian (- - -); fluid (–·–·–).

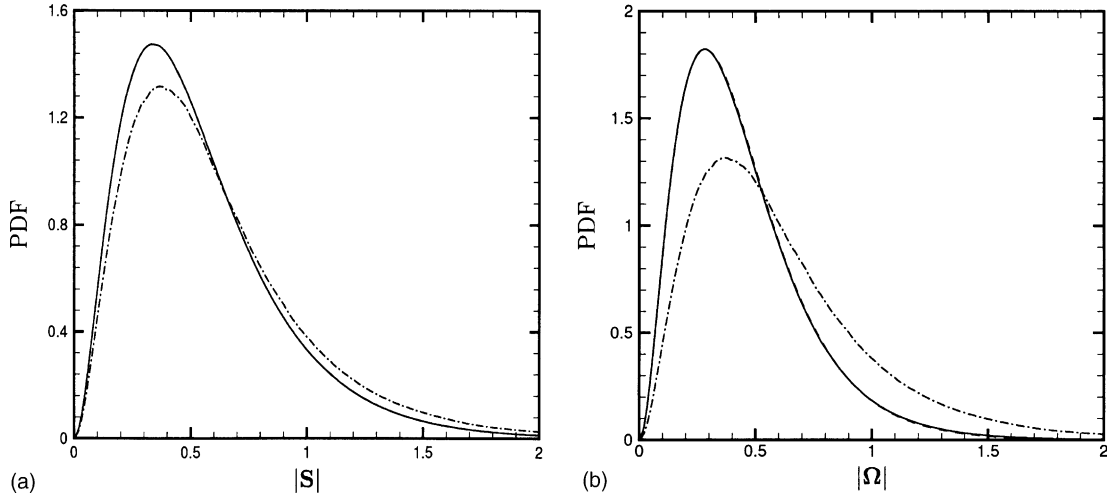

Fig. 12. Temporally and spatially averaged PDFs of $|\mathbf{\Omega}|$ for (a) $\tau_p = 0.1$ and $|\mathbf{V}_s| = 4$, (b) $\tau_p = 0.4$ and $|\mathbf{V}_s| = 0.5$. Lagrangian (—); equilibrium Eulerian (- - -); fluid (–·–·–).

$|\mathbf{V}_s| = 0.5$, the equilibrium Eulerian approach provides a good approximation to the Lagrangian tracking of particles.

The time-averaged mean vertical velocity of the particle, $\overline{\langle v_1 \rangle_p}$ is shown in Fig. 13(a) for the different cases considered. The corresponding time and particle-averaged mean vertical velocity of the fluid seen by the particles, $\overline{\langle u_1 \rangle_p}$ (not shown here), is simply smaller by the settling velocity $|\mathbf{V}_s|$. It is clear from Fig. 13(a) that the equilibrium Eulerian approximation provides a good approximation to the settling velocity of the actual Lagrangian particles.

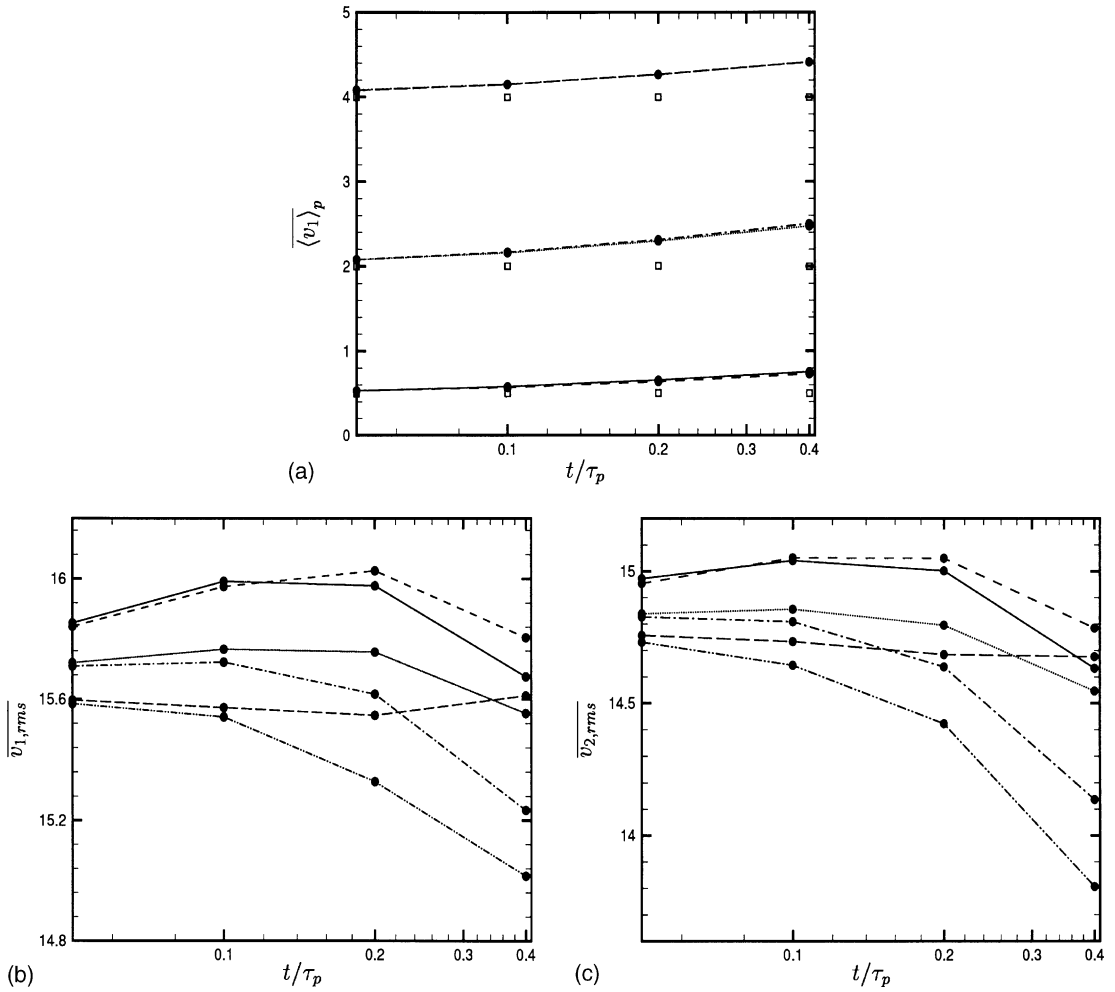

Fig. 13. Variation of (a) $\overline{\langle v_1 \rangle_p}$ (b) $\overline{v_{1,\mathrm{rms}}}$, (c) $\overline{v_{2,\mathrm{rms}}}$, with $\mathbf{V}_s$ and τ_p. Lagrangian (—) and equilibrium Eulerian (- - -) for $\mathbf{V}_s = 0.5$; Lagrangian (– · – · –) and equilibrium Eulerian (· · ·) for $\mathbf{V}_s = 2$; Lagrangian (– ¨ – ¨ –) and equilibrium Eulerian (- - -) for $\mathbf{V}_s = 4$; still-fluid settling velocity (square).

As shown by Wang and Maxey (1993), over the range considered, the settling velocity increases with τ_p. The influence of turbulence will decrease for particles of much larger τ_p. However, for such large particles, the equilibrium Eulerian expansion will cease to provide a good approximation. Fig. 13(b) and (c) shows the dependence of time-averaged rms vertical and horizontal velocity fluctuations of the particles on particle time scale and settling velocity. Note that the range of the vertical scale in these plots is quite narrow and therefore, the difference between the equilibrium Eulerian and the Lagrangian is small for all cases considered. Even for the worst case of $\tau_p = 0.4$ and $|\mathbf{V}_s| = 0.5$, the difference in rms vertical velocity fluctuation is less than 4% and for the smallest particle the difference is about 0.1% or less.

The PDFs of v_1 obtained from both the Lagrangian and Eulerian approaches are shown in Fig. 14 for the two cases $\tau_p = 0.1$, $|\mathbf{V}_s| = 4.0$ and $\tau_p = 0.4$, $|\mathbf{V}_s| = 0.5$. The PDFs cover a wide range of

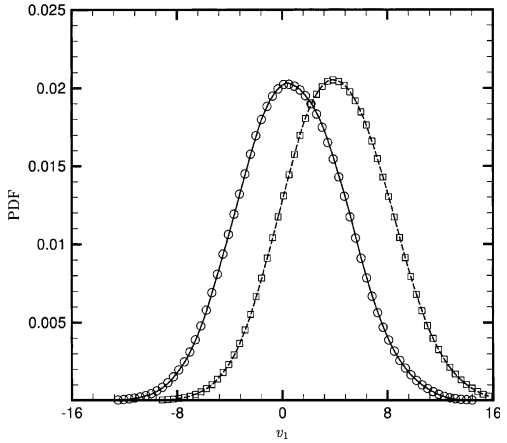

Fig. 14. Temporally and spatially averaged PDFs of v_1, for $\tau_p = 0.1$, $\mathbf{V}_s = 4$: Lagrangian (– – –); equilibrium Eulerian (square) and $\tau_p = 0.4$, $\mathbf{V}_s = 0.5$: Lagrangian (—); equilibrium Eulerian (circle).

vertical velocity taken by the settling particles and over this entire range, the Lagrangian and Eulerian PDFs virtually lie on one another. This is consistent with the good agreement between the equilibrium Eulerian and Lagrangian results of the mean and rms seen in Fig. 13(a) and (b). The good agreement between the PDFs in fact shows that it is not only the mean and the rms, but the entire distribution of the Lagrangian particle velocities is well reproduced by the equilibrium Eulerian approach, for all the cases considered.

4. Conclusions

The current work successfully demonstrates the application of the equilibrium Eulerian approach (Ferry and Balachandar, 2001) to the evolution of Eulerian particle concentration field over long periods of time. The Eulerian particle velocity field computed by the equilibrium Eulerian approach is used to evolve the particle concentration field, $\phi(\mathbf{x}, t)$. Thus, the need to solve three additional pdes for the Eulerian particle velocity field is obviated in the current approach and only the particle concentration equation needs to be solved. Here, it is observed that the inclusion of a spectral vanishing viscosity term is necessary to keep the solution bounded. This was done in a manner so as to preserve the spectral accuracy.

The Eulerian concentration field is then used as the weighting factor in calculating the particle-averaged Eulerian statistics. These are compared against the corresponding Lagrangian statistics obtained by tracking a large distribution of particles over long periods of time. In the current work, 12 different types of particles, involving four different dimensionless particle response time, τ_p, and three different dimensionless still-fluid settling (or terminal) velocity, $\mathbf{V}_s$, are considered. In all the cases considered, the time history of both the Lagrangian and the equilibrium Eulerian particle-averaged statistics showed good agreement. In particular, both these statistics showed rapid initial transience and an eventual statistically stationary state. Temporal averaging is then carried out in the statistically stationary state.

The time- and particle-averaged statistics of preferential concentration showed good agreement between the equilibrium Eulerian and the *exact* Lagrangian approaches. The difference between the two increased with increasing particle time scale, with the equilibrium Eulerian approximation tending to somewhat overpredict the degree of preferential accumulation of particles. The statistics on particle settling such as, mean settling velocity, rms vertical and horizontal particle velocity fluctuations and particle velocity (PDF), computed with both the equilibrium Eulerian and Lagrangian approaches, show good agreement.

In the context of the present spectral simulations, the introduction of the spectral vanishing diffusivity is crucial in obtaining meaningful concentration fields. The added diffusivity is targeted towards the high wavenumbers and by smoothening the sharp concentration gradients, it avoids local high wavenumber oscillations arising from Gibb's phenomenon (Canute et al., 1988). Although the influence on low wavenumber spectral behavior cannot be completely avoided, the value of spectral vanishing viscosity can be chosen to minimize the influence on large scale concentration variation. The present results are equally applicable in the context of finite difference and finite volume treatment of the particulate phase. Here again, with the use of equilibrium Eulerian approximation for the particle velocity, only the concentration field needs to be solved. In the finite difference and finite volume framework, a large body of literature on total variation diminishing (TVD) and essentially non-oscillatory (ENO) schemes is available, which can be efficiently employed for the evolution of the concentration field.

Acknowledgements

This research was supported by the Center for Simulation of Advanced Rockets at the University of Illinois, which is funded by the US Department of Energy through the University of California Subcontract number B341494. We gratefully acknowledge the isotropic turbulence code provided by Prof. Martin Maxey of Brown University.

References

Canute, C., Hussaini, M.Y., Quarteroni, A., Zang, T.A.., 1988. Spectral Methods in Fluid Dynamics. Springer-Verlag.

Druzhinin, O.A., 1995. On the two-way interaction in two-dimensional particle-laden flows: the accumulation of particles and flow modification. J. Fluid Mech. 297, 49–76.

Druzhinin, O.A., Elghobashi, S., 1998. Direct numerical simulations of bubble-laden turbulent flows using the two-fluid formulation. Phys. Fluids 10, 685–697.

Druzhinin, O.A., Elghobashi, S., 1999. On the decay rate of isotropic turbulence laden with microparticles. Phys. Fluids 11, 602–610.

Eswaran, V., Pope, S.B., 1988a. An examination of forcing in direct numerical simulations of turbulence. Comput. Fluids 16, 257–278.

Eswaran, V., Pope, S.B., 1988b. Direct simulations of the turbulent mixing of a passive scalar. Phys. Fluids 31, 506–520.

Ferry, J., Balachandar, S., 2001. A fast Eulerian method for disperse two-phase flow. Int. J. Multiphase Flow 27, 1199–1226.

Ferry, J., Balachandar, S., 2002. Equilibrium expansion for the Eulerian velocity of small particles. Powder Technol. 125, 131–139.

Gottlieb, D., Hesthaven, J.S., 2001. Spectral methods for hyperbolic problems. J. Comput. Appl. Math. 128, 83–131.

Karamanos, G.-S., Karniadakis, G.E., 2000. A spectral vanishing viscosity method for large-eddy simulations. J. Comput. Phys. 163, 22–50.

Maxey, M.R., 1987. The gravitational settling of aerosol particles in homogeneous turbulence and random flow fields. J. Fluid Mech. 174, 441–465.

Tadmor, E., 1989. Convergence of spectral methods for nonlinear conservation laws. SIAM J. Numer. Anal. 26, 30–44.

Wang, L.-P., Maxey, M.R., 1993. Settling velocity and concentration distribution of heavy particles in homogeneous isotropic turbulence. J. Fluid Mech. 256, 27–68.